COMPARISON OF LASER AND LIGHT EMITTING DIODE ILLUMINATION
FOR HIGH RESOLUTION BRIGHT-FIELD MICROSCOPY

A THESIS SUBMITTED TO

THE FACULTY OF ARCHITECTURE AND ENGINEERING

OF

EPOKA UNIVERSITY

BY

ALBERT KOPACI

IN PARTIAL FULFILLMENT OF THE REQUIREMENTS

FOR

THE DEGREE OF MASTER OF SCIENCE

IN

COMPUTER ENGINEERING

JULY  2022

**Approval sheet of the Thesis**

This is to certify that we have read this thesis entitled **"Comparison of laser and light emitting diode illumination for high resolution bright-field microscopy"** and that in our opinion it is fully adequate, in scope and quality, as a thesis for the degree of Master of Science.

_____

Dr. Arban Uka
Head of Department
Date: 07, 12, 2022

Examining Committee Members:

Assoc. Prof. Dr. Carlo Ciulla  (Computer Engineering)  _____

Dr. Arban Uka            (Computer Engineering)  _____

Dr. Shkëlqim Hajrulla        (Computer Engineering)  _____

**I hereby declare that all information in this document has been obtained and presented in accordance with academic rules and ethical conduct. I also declare that, as required by these rules and conduct, I have fully cited and referenced all material and results that are not original to this work.**

Name Surname: Albert Kopaci

Signature: _____

# ABSTRACT

## COMPARISON OF LASER AND LIGHT EMITTING DIODE ILLUMINATION FOR HIGH RESOLUTION BRIGHT-FIELD MICROSCOPY

Albert Kopaci

M.Sc., Department of Electronic and Digital Communication Engineering

Supervisor: Dr. Arban Uka

Medical Imagery, the most popular and challenging imagery techniques which have been a point of interest for many studies nowadays. Light microscopy requires proper illumination to acquire gigapixel high resolution and wide field of view images at the same time. Whereas incandescent light was once the only source of illumination, nowadays specialized light sources, such as laser emitting diodes (LED), lasers or arc lamps, are now being used. Light-emitting diodes (LEDs) have evolved into a serious option for practically all types of illumination in light microscopy due to their great efficiency and brightness. They are long-lasting, require no expensive electronics, and can be switched in nanoseconds. Aside from that, they have a narrow bandwidth and are available across the UV/Vis/NIR spectrum. As a result, they seem to be the most suitable illumination for different microscopy techniques. With a color temperature spanning from 2,600 to 5,000 K, the white LED is best choice for bright-field illumination, with the added benefit of being energy efficient.

On the other hand, lasers produce dense packets of monochromatic light that are extremely collimated and coherent, resulting in a tight beam with a very low rate of expansion. The extremely pure wavelength ranges emitted by the laser have a bandwidth and phase relationship that is unequalled by tungsten-halogen or arc-discharge lamps when compared to other light sources. As a result, laser light beams can travel long distances and be expanded to span apertures or concentrated to a very small, bright spot, which reduces diffraction and maintain the light intensity. In this

work we will explain in detail the differences between them using blind image quality assessments.

# ABSTRAKT

## KRAHASIMI I NDRICIMIT ME LASER DHE DIODAVE QË LËSHOJNË DRITË PËR IMAZHERINË ME FUSHË TË BARDHË DHE REZOLUCION TË LARTË

Kopaci, Albert

Master Shkencor, Departamenti i Inxhinierisë Elektronike dhe Komunikimit Dixhital

Udhëheqësi: Dr. Arban Uka

Imazheria Mjekësore, përfshin teknikat më të njohura dhe sfiduese të imazherisë të cilat kanë qenë një pikë interesi për shumë studime në ditët e sotme. Mikroskopia kërkon ndriçimin e duhur për të marrë imazhe me rezolucion të lartë gigapiksel dhe një fushë të gjerë shikimi në të njëjtën kohë. Ndërsa drita inkandeshente dikur ishte burimi i vetëm i ndriçimit, sot po përdoren burime të specializuara të dritës, si diodat që lëshojnë dritë (LED), lazerët ose llambat me hark. Diodat që lëshojnë dritë (LED) kanë evoluar në një opsion i shumë përdorur për të gjitha llojet e ndriçimit në mikroskopi për shkak të efikasitetit dhe shkëlqimit të tyre të madh. Ato janë të qëndrueshme, nuk kërkojnë pajisje elektronike të shtrenjta dhe mund të ndërrohen në nanosekonda. Përveç kësaj, ato kanë një gjerësi bande të ngushtë dhe janë të disponueshme në të gjithë spektrin UV/Vis/NIR. Si rezultat, ato duket se janë ndriçimi më i përshtatshëm për teknika të ndryshme mikroskopike. Me një temperaturë ngjyrash që shtrihet nga 2,600 në 5,000 K, LED i bardhë është zgjidhja më e mirë për ndriçimin në fushë të ndritshme, me përfitimin e shtuar të të qenit efikas në energji.

Nga ana tjetër, lazerët prodhojnë paketa të dendura drite monokromatike që janë jashtëzakonisht të lidhura dhe koherente, duke rezultuar në një rreze të ngushtë me një shkallë shumë të ulët zgjerimi. Gama e gjatësisë valore jashtëzakonisht të pastër të emetuar nga lazeri ka një lidhje gjerësie brezi dhe faze që është e pabarabartë nga llambat tungsten-halogjen ose hark-shkarkuese kur krahasohen me burimet e tjera të

dritës. Si rezultat, rrezet e dritës lazer mund të udhëtojnë në distanca të gjata dhe të zgjerohen për të shtrirë hapjet ose të përqendrohen në një pikë shumë të vogël dhe të ndritshme, e cila redukton difraksionin dhe ruan intensitetin e dritës. Në këtë punim do të shpjegojmë në detaje dallimet ndërmjet tyre.

*Fjalët kyçe:* *Diodat që lëshojnë dritë, Ndriçimi me lazer, Brightfield mikroskopi, Apertura, Gjerësia e bandës, Rreze drite.*

# Table of Contents

# LIST OF TABLES

# LIST OF FIGURES

# CHAPTER 1

# INTRODUCTION

## 1.1    Medical Imagery

Medical image processing is an important technology which plays an important role in monitoring, diagnosing, and treating medical problems. Medical imaging is ranked as one of the top medical development technologies over the years. This technique of diagnosing has helped evolution of treating disease noninvasively. Monitoring of disease as cancer has helped a lot of people diagnosing and curing it in early stages. Medical imaging is helping doctors to detect cancer in size of a rice. On the other hand, combining it with other technological development as Artificial Intelligence is detecting diseases which doctors cannot distinguish with naked eyes. As we mentioned early the technology of diagnosing and medical imaging is improving every day. Image quality becomes sharper and clearer, diagnosing methods have evolved and images provide a vast of information into a comprehensive format in most efficient way.

As we know medical imagery is a very wide field used in clinical, laboratories, diagnosis, and monitoring but common types of it includes:

- X-rays

- CT (computed tomography) scan

- MRI (magnetic resonance imaging)

- Ultrasound

- Nuclear medicine imaging, including positron-emission tomography (PET)

These techniques use a technology which is optimized for achieving a goal. They differ in how they show the information what is happening in certain cases of diseases.

Overall medical imaging has changed many people's lives for better helping diagnoses and treatments by greatly reducing the amount of guess work done by doctors allowing them to deal with patient injuries more efficiently.

## 1.2    Image Quality Assessment

Image Quality Assessments algorithms have been developed to determine the characteristics of an image for a given purpose. In the beginning there were developed IQA (Image Quality Assessments) algorithms which determine the quality of an image ang its metrics related to: illumination, sharpness, contrast, magnification, and resolution. Later, these techniques were used in medicine for diagnostic purposes which have emerged more recently (especially to epidemiological studies). Nowadays these techniques are combined with deep learning techniques to diagnose various disease.

There are two main algorithms used in IQA to determine the metrices of an image to conclude a score corresponding to its resolution. Different from human eye which evaluate the image subjectively for example by stating that resolution for a given image may be good, bad, very good, very low etc. these algorithms aim to equalize this resolution score with a value which is concluded by evaluating its metrices, we may say that a low resolution image has a score of 10, another with a better quality has a score of 30 and the best resolution has a score of 100. Therefore, we avoid subjective scoring. One type of IQA techniques is those which use reference image to determine the quality of others, and the other one is called no reference or blind image quality assessments. We will discuss different types of these techniques which uses deep learning algorithms to calculate weights and scores for an image.

## 1.3 Extended field of view reconstruction in Fourier ptychographic microscopy

Nowadays, microscopy technique is one of the most popular and challenging studies around the world. The main porpoise of this studies is to achieve high image qualities using alternative microscopes and techniques that provides us the same or better results than professional microscopes. This thesis focuses on two methods that are widely used to improve analysis quality of cell using bright field microscopes. These techniques are called vignetting effect and digital refocusing, it also includes extending depth of field (DOF) in Fourier reconstruction. In perspective of geometrical optics is easy to understand vignetting effect but how this affect the image quality and reconstruction from perspective of wave optics is unexplored. In FPM microscopes with low magnification objective and large FOV, the linear space-invariant (LSI) model is destroyed by diffraction at the stops or apertures associated with different lenses called vignetting. Two common and most used solutions of this effect are: Dividing FOV into smaller patches and removing imperfect segments to maintain the consistency of FPM. Regarding digital refocusing, an auto focus system increments both size and cost and can debase optical execution by misalignment.

## 1.4    Motivation

The aim of this paper is to evaluate the quality of images which are captured by an autonomous conventional microscope with autofocus algorithms increased resolution and high field of view (FOV) compared to commercial microscopes. Sample is placed on microscope table and then just by initializing the process autonomous microscope which is programmed with LabView will move in that position where sores for image focus are the highest. These are evaluated using MATLAB metrices which determine the focus zone of an image. After that the most in focus image is captured. There are different conditions which affect the image and then its resolution. All combination which includes the following conditions will be considered to enhance the technique and achieve gigapixel images. We will combine Led illuminated images (including following color: white, red, blue green, yellow, purple, light/dark green, light/dark blue and light/dark red), Laser illumination (including following colors: green, red), both techniques with diffuser and without it.

## 1.5    Thesis Structure

Thesis is organized into 5 chapters. The first chapter gives an overview of the field of study, scope, and the motivation of the work. The second chapter is about literature review. We will start with IQA and Deep Learning Algorithms to continue with the specific technique and code which is used in this work. The third chapter is about the methodology of the work and experiments that are done. The fourth chapter is about the results gotten from the third chapter experiments. The fifth chapter is about conclusions.

# CHAPTER 2

# LITERATURE REVIEW

## 2.1    Introduction

In this chapter we are going to see some of the techniques used on IQA Algorithms. How these algorithms combined with Deep Learning trains datasets and then predicts weight to evaluate image quality in a subjective way different and more specifically than human evaluation. We also will mention how these techniques can be applied to our autonomous microscope for high quality imagery scoring.

## 2.2    Regional-Adaptive Deformable Network for IQA

Image Quality Assessment (IQA) aims to assess the perceptual quality of images in a manner that is consistent with human subjective perception. However, the existing IQA methods yield unsatisfactory performance on distortions (such as spatial shift and texture noise) introduced by generative adversarial networks (GAN). A method is proposed to overcome this problem, called "reference-oriented deformable convolution", which solves the issues faced by current IQA methods, because of their low tolerance to spatial misalignment.

Other proposed solutions include a patch-level attention module, a modified residual block, and a Region-Adaptive Deformable Network (RADN). The first serves to enhance the interaction among different patch regions, while the second to construct a patch-region-based baseline called WResNet.
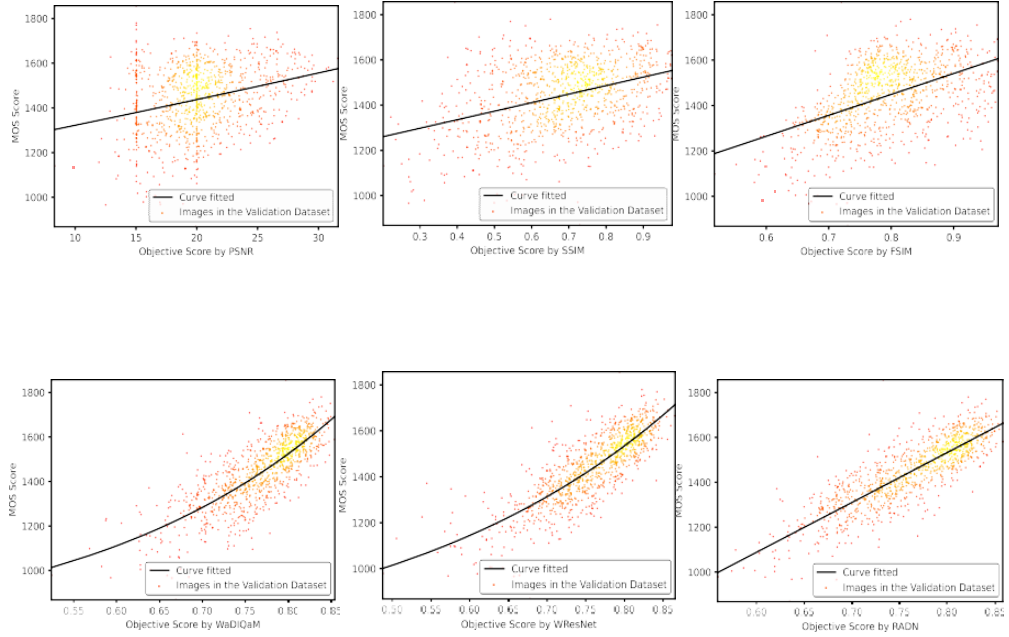
***Figure 1***. Scatter plots of IQA models. MOS labels and Predicted scores.[1]

Image quality assessment tasks have the goal of assessing image perceptual quality like humans. Although current IQA methods have shown to maintain consistency with human subjective evaluation, they also exhibit some limitations. The existing algorithms cannot distinguish GAN-generated image textures from noises and natural details. For this reason, a new IQA benchmark has been proposed, as well as a Space Warping Difference (SWD) layer to compare the features on a small range around the corresponding position. This operation, although robust to spatial shifts, lacks flexibility and is limited to specific contexts. To deal with the drawbacks mentioned before, the Region-Adaptive Deformable Network (RADN) has been proposed. The baseline WResNet is built using the modified residual blocks.

For adaptation to images of significant differences, a novel module called "reference-oriented deformable convolution" is proposed. Applying this method to distorted images can refer images interact with the distorted ones and, as a result, be robust to the distortion introduced by generative adversarial networks.

Furthermore, a patch-level attention mechanism is proposed to boost the information interactions among the patch regions. This, along with other processes, tries to improve the information interaction across distinct patches to get more accurate picture feature expressions. IQA algorithms are used to assess the quality of photos that may have been degraded during the processing process. General quality assessment algorithms that resemble human subjective judgment have been developed through research. A patch-level attention has been adopted combined with reference-oriented deformable convolution to handle GAN-based distorted images in a dataset.

Deformable convolution. Has been proven to be effective for sophisticated vision tasks such as object detection and semantic segmentation. It also performs well in low-level vision asks such as video super-resolution and video deblurring. Reference-oriented deformable convolution has been adopted for FR-IQA (Full Reference IQA).

Attention mechanism. Attention mechanisms have been widely used in various tasks.
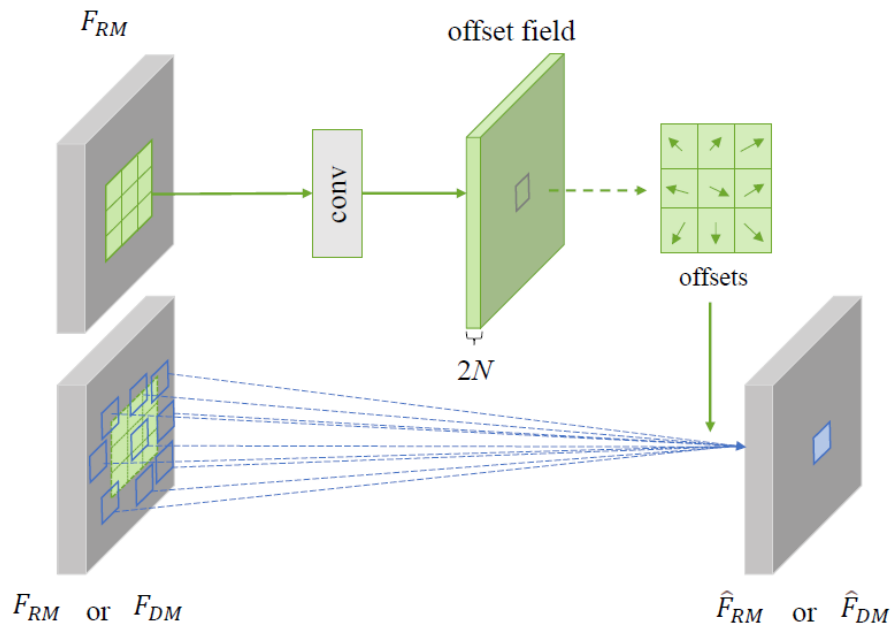


*Figure 2*. Reference-oriented deformable convolution. FRM and FDM indicate the feature map.[1]

7
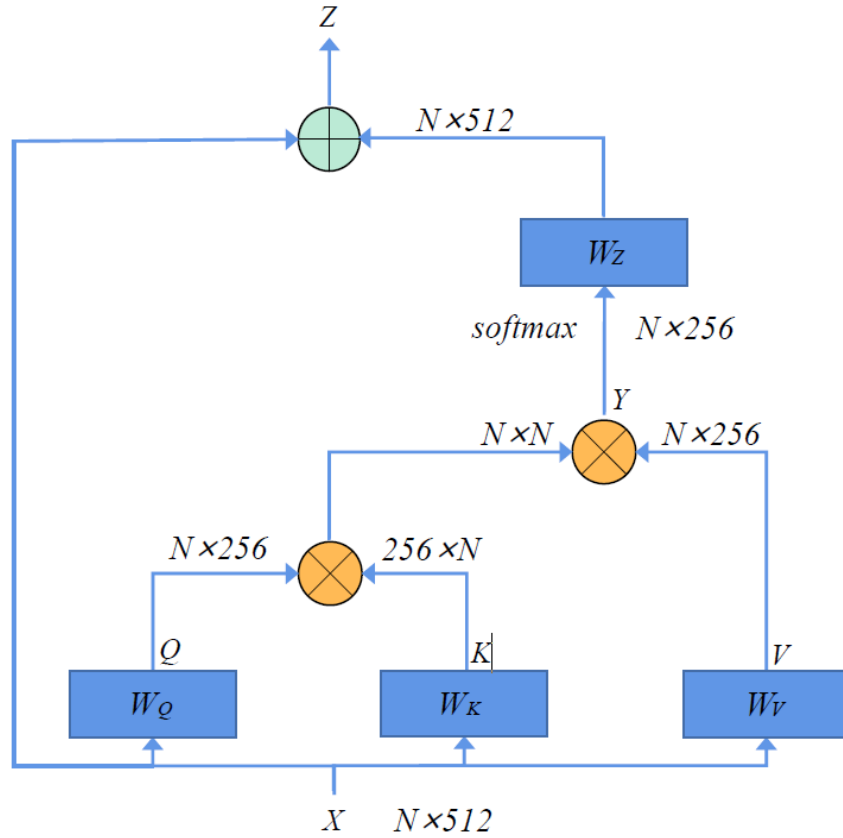
*Figure 2* *The patch-level attention block. The feature maps are shown as the shape of their tensors, and N is the number of patches.*[1]

A pair of images (reference image, distorted image) are cropped into patches, and a series of operations is performed on them. Considering the characteristics of IQA tasks and the dataset used, the performance of the classic residual block is improved with a more reasonable structure. The modified residual blocks are used to build a baseline method named WResNet (where W stands for weighted averaging). With the application of this reference-oriented deformable convolution is both reference and distorted branches, the model can deal with GAN-based distortion better and learn the spatial shift-invariant features from the paired images adaptively. Contrastive training

is an acceptable wat to take advantage of the labels from the side, given that the MOS labels are obtained by manually comparing the image pairs. Training details. The proposed model is trained with a certain patch-based training strategy. For training, random samples of 32 patches have been taken from per distorted image and its corresponding reference image rather than the whole image. For testing, each pair of images are cropped into a certain number M of nonoverlapping patches. These patches are then fed into the network to predict the weight and score of each patch. The final quality score is calculated as a weighted average of all scores. Data arrangement for contrastive pretraining. Considering the gap among various images, distorted images have been collected corresponding to the same reference and from the same category for contrastive pretraining. Images from the same contrast group have been arranged into one batch to avoid the duplicate score computing process.

The models have been compared with the state-of-the-art FR-IQA methods on the NTIRE 2021 IQA challenge validation and testing datasets. In general, deep learning-based methods achieved better performance than the traditional methods. To make it easier to understand the effectiveness of the method used, the weights of patches in some images are visualized. Compared with WResNet, the whole RADN model pays less attention to the regions with less informative or the texture-less regions. For images of different content, RADN perceives the images better and observably stays under human's perception. Despite the diversity and the severe GAN-based distortions, RADN yields satisfactory results.

## 2.3 MS-UNIQUE: Multi-model and Sharpness-weighted Unsupervised Image Quality Estimation

Multi-model and Sharpness-weighted Unsupervised Image Quality Estimation describes the usage of independent linear decoder trained models to estimate the

perceived quality of images. The training is carried out on 100,000 image patches from the ImageNet database using unsupervised learning. The perception of the quality of an image is calculated objectively and this process can be automated using Image Quality Assessment (IQA). This focuses on making advancements in the FR model, which requires the original image for predicting the quality of the distorted image, proposed.[2] The already build model is called UNIQUE, it consists of a shallow learning architecture with 1 hidden layer using sparsity criterion. The proposed advancement is to improve performance through analyzing the weights learned and utilizing the importance of sharpness in measuring quality. The filters used to estimate the quality of an image are the weights calculated using a linear decoder. These filters are also separated into 2 groups, the first one captures edges or sharpness, and the second captures color, and this paper focuses more on sharpness filters. The images are firstly transformed into YHCr color space. They found that using a combination of luminance, green and chroma brings the best results. The model starts with 1,000 images retrieved from the ImageNet2013 dataset. After changing the color space, the authors extract randomly 100 patches with size 8x3x3 from each image. Each patch is reshaped to a column vector and the result is a 192x100000 input patch matrix (10000 patches with 192 input features each).[3] The adjacent features in the input features are then decorrelated using Zero Component Analysis (ZCA) to reduce redundancy. The authors didn't change the structure of the model, meaning that it still is an unsupervised neural network framework with one hidden layer. The weights and bias are randomly initialized and adjusted iteratively. The response of the hidden layer is given by the formula

$$\boldsymbol{s} = \boldsymbol{sigmoid}(\boldsymbol{W_1^T} * \boldsymbol{P} + \boldsymbol{b_1}) \qquad \text{(Equation 1)}$$

Sigmoid is used as an activation function to introduce non-linearity in the model. These hidden layer responses are filtered using another set of weights to obtain back a reconstructed version of the input.

$$\boldsymbol{P} = \boldsymbol{W_2^T} * \boldsymbol{s} + \boldsymbol{b_2} \qquad \text{(Equation 2)}$$

10

We initially set the number of neurons in the hidden layer to 81 and trains the model for 400 epochs. The process is repeated for greater number of neurons in the hidden layer. Increasing the number of neurons increases the sparsity on the patches, assuring that we have multiple filters learned from sparsely or compactly representing the images. The responses we get from this model are weighted based on the sharpness characteristics of corresponding filters. The edge filter response is given in higher weightage of 2 while the color responses are lowered by a weight of 0.5. And this process is repeated for various number of neurons in the hidden layer. The responses in feature vector that are significantly less than the average activation value set during training are assigned a zero to mimic the suppression mechanisms in the HVS (used for differentiating between sharp and color filters). The feature vectors corresponding to the original and distorted images are compared using the 10th power of Spearman correlation coefficient to fully utilize the quality estimation range. The quality estimator is validated using LIVE image quality and TID 2013 databases. The databases have more than 3500 distorted images divided into 7 different categories based on distortion type. The performance was evaluated using root mean squared error, outlier ratio, Pearson, and Spearman correlation coefficients. The model was also compared to 11 other popular quality assessment methods and the results are shown in the table below.

Table 1. Performance of image quality estimators.[2]

| Methods | PSNR | PSNR HA [10] | PSNR HMA [10] | SSIM [4] | MS SSIM [11] | CW SSIM [12] | IW SSIM [13] | SR SIM [14] | FSIMc [15] | PerSIM [16] | UNIQUE [1] | MS-UNIQUE |
|---|---|---|---|---|---|---|---|---|---|---|---|---|
| **Outlier Ratio** | | | | | | | | | | | | |
| **TID 13** | 0.725 | 0.615 | 0.670 | 0.732 | 0.697 | 0.855 | 0.700 | 0.632 | 0.727 | 0.655 | 0.640 | **0.611** |
| **Root Mean Square Error** | | | | | | | | | | | | |
| **LIVE** | 8.61 | 6.93 | **6.58** | 7.52 | 7.43 | 11.2 | 7.11 | 7.54 | 7.20 | 6.80 | 6.76 | 6.61 |
| **TID 13** | 0.87 | 0.65 | 0.69 | 0.76 | 0.68 | 1.20 | 0.68 | 0.61 | 0.68 | 0.64 | 0.60 | **0.57** |
| **Pearson Correlation Coefficient** | | | | | | | | | | | | |
| **LIVE** | 0.928 | 0.953 | **0.958** | 0.945 | 0.946 | 0.872 | 0.951 | 0.945 | 0.950 | 0.955 | 0.956 | **0.958** |
| **TID 13** | 0.705 | 0.850 | 0.827 | 0.789 | 0.832 | 0.227 | 0.831 | 0.866 | 0.832 | 0.854 | 0.870 | **0.884** |
| **Spearman Correlation Coefficient** | | | | | | | | | | | | |
| **LIVE** | 0.909 | 0.937 | 0.944 | 0.949 | 0.951 | 0.902 | **0.960** | 0.955 | 0.959 | 0.950 | 0.952 | 0.949 |
| **TID 13** | 0.700 | 0.847 | 0.817 | 0.741 | 0.785 | 0.562 | 0.777 | 0.807 | 0.851 | 0.853 | 0.860 | **0.870** |

*Table 2 Distributional difference between subjective scores and objective estimates.*

| Metric | Difference-LIVE | | | | | Difference-TID13 | | | | |
|---|---|---|---|---|---|---|---|---|---|---|
| | EMD | KL | JS | HI | L2 | EMD | KL | JS | HI | L2 |
| **PSNR-HMA** | 0.226 | 0.205 | 0.053 | 0.226 | 0.066 | 0.360 | 0.927 | 0.117 | 0.360 | 0.124 |
| **IW-SSIM** | 0.297 | 0.325 | 0.072 | 0.297 | 0.076 | 0.500 | 1.678 | 0.196 | 0.500 | 0.180 |
| **UNIQUE** | 0.236 | 0.258 | 0.055 | 0.236 | 0.069 | 0.386 | 0.855 | 0.120 | 0.386 | 0.109 |
| **MS-UNIQUE** | **0.209** | **0.176** | **0.038** | **0.209** | **0.057** | **0.357** | **0.734** | **0.108** | **0.357** | **0.103** |

## 2.4 Blind Image Quality Assessment Using a Deep Bilinear Convolutional Neural Network

This paper focuses on creating a deep bilinear CNN model for a no-reference or blind image quality assessment. The bilinear model is used to differentiate between synthetic and authentic distortions of images. For synthetic distortions, the authors construct a large-scale pretraining set based on Waterloo Exploration Database and PASCAL VOC Database where the images are synthesized with 9 different distortions and 2-5 distortion levels. For authentic distortions, the authors use a pre-trained CNN from ImageNet that contains many realistic natural images of different perceptual quality.[3] These 2 CNNs are unified into a representation for final quality prediction.

### 2.5.1 CNN for Synthetic Distortions

As before mentioned, the databases used are Waterloo Exploration Database and PASCAL VOC Database. In total, the authors have 21,869 source images and to these, they apply 9 distortion types, namely: Gaussian blur, White Gaussian noise, JPEG compression, JPEG2000 compression, Contrast stretching, pink noise, Image color quantization with dithering, Over-exposure, and Under-exposure. The images

are synthesized with five distortion levels except for over-exposure and under-exposure where only 2 levels are generated. As result, the pre-training set contains 852,891 distorted images. The authors pre-train a CNN to classify distortion types and degradation level which offers meaningful initialization of the network. The ground truth is formed as an M-class indicator using the distortion type and level. Since they're using 7 distortion types with 5 levels and 2 distortion types with 2 levels, that leads to an M=39. The CNN architecture is inspired by VGG-16 and is shown in the picture below.



*Figure 3* *Convolutional layer structure*

The image size is 224 x 224 x 3 and the convolution kernel size is 3 x 3 with a stride of 2 to reduce the spatial resolution. The features are padded with zeros and the non-linear activation function is ReLU. The SoftMax is computed as:

$$\hat{p}_k^{(i)}(X^{(i)}; W_s) = \frac{\exp\left(y_k^{(i)}(X^{(i)}; W_s)\right)}{\sum_{j=1}^{M} \exp\left(y_j^{(i)}(X^{(i)}; W_s)\right)} \qquad \text{(Equation 8)}$$

and the cross-entropy loss as:

$$l_s(\{X^{(i)}\}; W_s) = -\sum_{i=1}^{N} \sum_{j=1}^{M} p_j^{(i)} \log \hat{p}_j^{(i)}(X^{(i)}; W_s) \qquad \text{(Equation 9)}$$

14

### 2.5.2    CNN for Authentic Distortions

For this CNN, the authors use an already built model because training a model to gain meaningful training data with a small number of samples leads to overfitting. The model to extract relevant features for authentically distorted images is the VGG-16 pre-trained for the image classification task on ImageNet.

These 2 CNNs are combined into a bilinear model, creating a DB-CNN. These models have been shown to be very effective in modeling two-factor varication, which in our case are synthetic and authentic distortions. The bilinear pooling is formulated as: $B = Y\_1^T Y\_2$ where Y1 and Y2 denote the first and second CNN respectively.[4] There are also no problems with combining the images since the CNN for synthetic distortions also has similar structure to VGG-16. For the empirical loss, the authors use the l2-norm since it has been widely used in previous studies.

The experiments are conducted in three singly distorted synthetic IQA databases, i.e., LIVE, CSIQ and TID2013, a multiply distorted synthetic dataset LIVE MD, and the authentic LIVE Challenge Database. The databases contain a wide variety of synthetic and authentic distortions on numerous pictures with different qualities. The images are randomly split into a train and test size with a ratio of 80 with 20%. The metrics to benchmark the model are Spearman rank correlation coefficient (SRCC) for prediction monotonicity and Pearson linear correlation coefficient (PLCC) for the prediction precision.

On individual databases, the DB-CNN model achieves superior performance compared to other IQA models but that's because the authors tweak the parameters for each database to get the best results. When tested on individual distortion types, the results are like other models and the authors notice that the BIQA models fail in three distortion types on TID2013. It is also worth mentioning that the model did a great job on distortions unseen on the training. When testing the performance across all databases, the model did better than the other IQA model in almost all databases.

## 2.5 Automatic image quality assessment

Automatic image quality assessment is essential in handling low quality images to obtain images with high perceptual quality. Deep learning is used a lot in blind image quality assessment. An important step in blind image quality assessment is feature identification which is done quite well by the deep learning algorithms. As all other methods these methods estimate image quality as the deviation from the Natural Scene Statistics Model. In this section we are going to see in detail the Deep Learning for BIQ assessment algorithm. This algorithm is relatively new and was proposed in 2017. Training an CNN by yourself is a hard process as big datasets are hard to find. Another approach to apply transfer learning, find an already trained CNN, and use it as feature extractor or initialization for the forwarding learning process.[5] This algorithm uses a trained Convolutional Neural Network, the Caffe neural network architecture as a feature extractor. Then an SVR (Support vector regression) with linear kernel is applied on top of it to map the CNN features to quality scores perceived. 4096 is the length of the feature vector. Below we show the architecture of the network.

| | conv1 | pool1 | norm1 | conv2 | pool2 | norm2 | conv3 | conv4 | conv5 | pool5 | fc6 | fc7 | fc8 |
|---|---|---|---|---|---|---|---|---|---|---|---|---|---|
| Type | Conv | MaxPool | LRN | Conv | MaxPool | LRN | Conv | Conv | Conv | MaxPool | FC | FC | FC |
| Kernel size | $11 \times 11$ | $3 \times 3$ | | $5 \times 5$ | $3 \times 3$ | | $3 \times 3$ | $3 \times 3$ | $3 \times 3$ | $3 \times 3$ | | | |
| Depth | 96 | | | 256 | | | 384 | 384 | 256 | | 4096 | 4096 | |
| Stride | 4 | 2 | | 1 | 2 | | 1 | 1 | 1 | 2 | | | |
| Padding | 0 | | | 2 | | | 1 | 1 | 1 | | | | |

*Figure 4* *Different strategies applied on DeepBiq*[5]

As stated on the publication of DeepBiq, for testing the network different strategies were used.

1- Different pretrained CNN were used

2- Different strategies were used for feature and score prediction pooling.

3- Fine Tunned CNN for category-based image quality assessment were used.

### 2.6.1  Experiments and Results

Experiments were done using three different CNN with same architecture trained by different dataset.[6]

•       ImageNet-CNN. 1.2 million images for object recognition of 1000 categories were used for training.

•       Places-CNN, here 2.5 million images were used for training. Images were from the Places database for scene recognition. In total there were 205 categories.

•       ImageNet + Places CNN composed of 3.5 million images of 1138 different categories was used for training. This dataset was obtained by merging two upper datasets.

CNN mostly require a fixed size of image. Science resizing the image would mask some artifacts a different design choice was considered, cropping the image. Image was cropped to its 21% from 500x500 to 227x227.  The final image quality is then obtained by processing the quality of each crop. Also, tests were done using a fine-tuned CNN. This is very usefully when the dataset is not very large. Using transfer learning proves to be an excellent choice on these cases. The authors replaced the last layer of trained CNN with random values. Then layer is trained from scratch and updated by back propagation. This new CNN is able now to classify image subregion into five classes based on IQA score. bad, poor, fair, good, and excellent. The design choices for DeepBIQ were compared with some of the leading assessment algorithms at the time which shows the incredible performance of deep BIQ.

To compare results the median LCC, SROCC and nMAE over the 10 train-test splits are reported. Below we show the tables of some of the experiments reported on paper2.

|  | Sub-reg | LCC | SROCC | nMAE |
|---|---|---|---|---|
| DIIVINE [33] |  | 0.57 | 0.52 | 0.14 |
| BRISQUE [30] |  | 0.61 | 0.61 | 0.13 |
| BLIINDS-II [39] | ✓ | 0.46 | 0.41 | 0.16 |
| S3 index [47] |  | 0.32 | 0.30 | 0.18 |
| NIQE [31] |  | 0.48 | 0.43 | 0.15 |
| C-DIIVINE [51] | ✓ | 0.67 | 0.65 | 0.12 |
| FRIQUEE [11,13] |  | 0.71 | 0.68 | 0.12 |
| HOSA [49] | ✓ | 0.74 | 0.72 | 0.10 |
| **DeepBIQ (Exp. I)** |  | 0.72 | 0.70 | 0.11 |
| **DeepBIQ (Exp. II)** | ✓ | 0.79 | 0.79 | 0.09 |
| **DeepBIQ (Exp. III)** | ✓ | **0.91** | **0.89** | **0.06** |

The best method is reported in bold

*Figure 5* *Deep BIQ comparing three approaches with ottter algorithms.*

| Method | Sub-reg | LCC | SROCC | nMAE |
|---|---|---|---|---|
| DIIVINE [33] |  | 0.90 | 0.88 | 0.16 |
| BRISQUE [30] |  | 0.93 | 0.91 | 0.12 |
| BLIINDS-II [39] | ✓ | 0.93 | 0.91 | 0.11 |
| Low Level Feat. [20] |  | 0.94 | 0.94 | 0.09 |
| Multitask CNN [19] |  | 0.93 | 0.94 | 0.09 |
| HOSA [49] | ✓ | 0.97 | 0.96 | **0.05** |
| **DeepBIQ** | ✓ | **0.97** | **0.96** | 0.06 |

The best method is reported in bold

*Figure 6* *Deep BIQ compare with other algorithms*

Most of the state-of-art BIQA methods learn estimation of image quality from human subjective scores. To take this to next step this section introduces research done by Wufeng Xue that tries to remove the human factor and make an algorithm that will learn by itself. The proposed method considers on clustering. It tries to identify a set of quality-aware centroids for BIQA. The algorithms only need some reference and distorted images to be trained. Human subjective scores are not necessary. Disported

images are generated by the reference images based on 4 types of distortions, Gaussian noise, Gaussian blur, JPEG compression and JPEG2000 compression. At the final step a dataset of 10 reference images and 120 distorted images is obtained. All possible combinations of distortions are used. Below we show the flowchart of the proposed method.
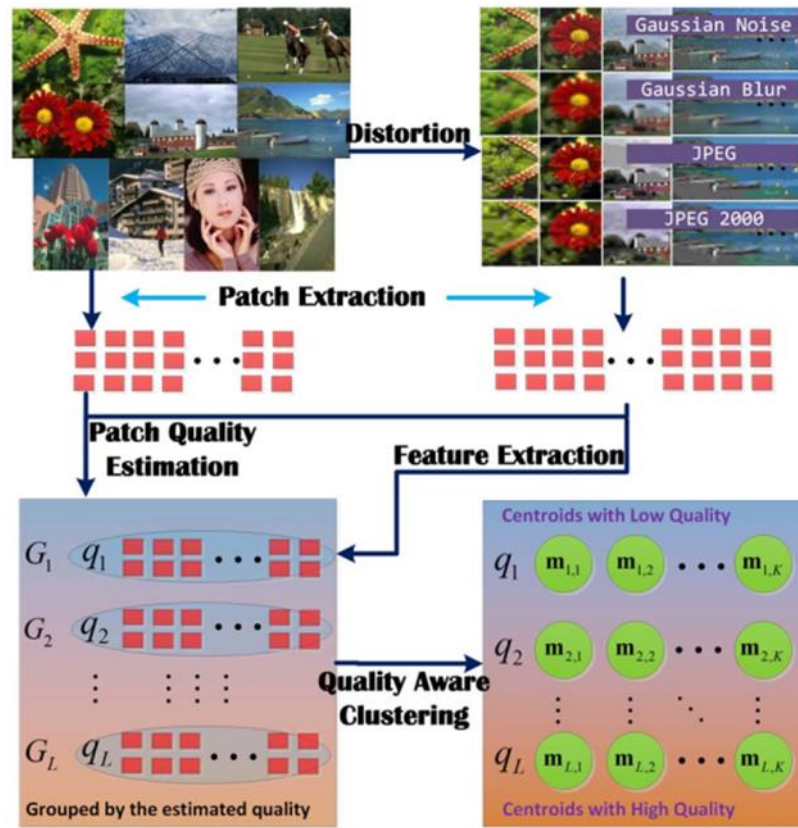


*Figure 7* *Flowchart of proposed BIQA*[7]

A full reference image quality assessment is used to assign a perceptual quality to the dataset images. Let xi be a patch of the distorted image and the di the corresponding patch of the reference image. The difference between the reference image and the corresponding distorted image is calculated using FSIM.

$$s_i = S(x_i, d_i) = \frac{2PC(x_i)PC(d_i)+t_1}{PC(x_i)^2+PC(d_i)^2+t_1} \; X \; \frac{2G(x_i)G(d_i)+t_2}{G(x_i)^2+G(d_i)^2+t_2} \qquad \text{(Equation 10)}$$

Where $PC(x_i)$ and $G(x_i)$ refer to phase congruence and $t_1$ and $t_2$ are constants of positive numbers.

The similarity score of the image is evaluated as the mean of all Si of an image. Si is normalized for it to be as close to s as possible. The formula below is used for the normalization donating that    *** OMEGA** is the set of patch indices of an image then:

$$C = \frac{\sum_{i\epsilon\Omega} s_i}{10 \sum_{i\epsilon\Omega p} s_i} \qquad \text{(Equation 11)}$$

The next step is quality aware clustering. Normalization of the patch quality in the previous step gives a set of patches and their quality scores. Then clustering is applied based on quality score. To enhance clustering accuracy in of each group the clustering method should be based on some mineral feature of di[8]. Researchers proposed a high pas filter to extract the feature of the patch di.

$$h_\sigma(r) = \mathbf{1}_{r=0} - \frac{1}{\sqrt{2\pi\sigma}} \exp\left(-\frac{r^2}{2\sigma^2}\right) \qquad \text{(Equation 12)}$$

Filter outputs of di are merged into a single feature vector as fi. Then the QAC of di from Gi is performed using K-Mean clustering algorithm.

$$min_{mi,k} \sum_{k=1}^{K} \sum_{di\epsilon G1,k} \lVert f_i - m_{i,k} \rVert^2 \qquad \text{(Equation 13)}$$

The next step is Blind Quality Pooling. The perceptual quality procedure is proceeded in this step. It is composed of two steps, patch partition and feature

extraction, cluster assignment on multiple quantity levels, patch quality score estimation, and final pooling of all patch's quality.

• Patch partition and feature extraction: High pas filter is used to extract features from the overlapped regions of patches.

• Cluster Assignment: In each cluster level we find the nearest centroid to the feature vector of the patch. Then the weighted average of the quality levels of these centroids expresses the quality of the patch.

• Patch Quality Estimation. This step is used to evaluate the quality of the patch. The final quality score is donated by the formula below.

$$z_i = \frac{\sum_{l=1}^{L} q_l \, exp(-\delta_{l,i}/\lambda)}{\sum_{l=1}^{L} exp(-\delta_{l,i}/\lambda)} \qquad (\text{Equation } 14)$$

• Final Pooling. With the evaluated quality of all patches then we can evaluate the quality of the image as arithmetic average of all patches.

The results of this algorithm were quite impressive. The network was trained by 29 images processed by 5 types of distortions producing a dataset of 779 images. Below we show the table with the results of the experiment.

| SROCC | Blind/FR | JP2K | JPEG | WN | GB | ALL |
|---|---|---|---|---|---|---|
| QAC | Blind | 0.8704 | 0.9126 | 0.8624 | 0.8483 | 0.8627 |
| PSNR | FR | 0.9361 | 0.8879 | 0.9363 | 0.9291 | 0.9218 |
| SSIM | FR | 0.9605 | 0.9543 | 0.8974 | 0.9608 | 0.9325 |
| FSIM | FR | 0.9685 | 0.9654 | 0.9262 | 0.9729 | 0.9616 |
| PCC | Blind/FR | JP2K | JPEG | WN | GB | ALL |
| QAC | Blind | 0.8822 | 0.9376 | 0.8735 | 0.8439 | 0.8768 |
| PSNR | FR | 0.927 | 0.7898 | 0.9438 | 0.9081 | 0.8463 |
| SSIM | FR | 0.8966 | 0.9165 | 0.8044 | 0.8692 | 0.8622 |
| FSIM | FR | 0.9073 | 0.9026 | 0.7642 | 0.8838 | 0.8795 |

*Figure 8* *Results comparing with other methods*[9]

The image below shows computational comparation of this method with other methods.

| BLIINDS-II [17] | Ratio of Samples for training | | | DIIVINE [14] | Ratio of Samples for training | | |
|---|---|---|---|---|---|---|---|
| | 80% | 50% | 30% | | 80% | 50% | 30% |
| LIVE | 0.9425 | 0.9198 | 0.8973 | LIVE | 0.8946 | 0.8768 | 0.7954 |
| CSIQ | 0.9003 | 0.8832 | 0.8465 | CSIQ | 0.8697 | 0.8246 | 0.7838 |
| TID2008 | 0.8982 | 0.8310 | 0.7690 | TID2008 | 0.8930 | 0.7902 | 0.7132 |
| Average | 0.9163 | 0.8851 | 0.8480 | Average | 0.8850 | 0.8369 | 0.7716 |
| CORNIA [27] | Proportion of Samples for training | | | BRISQUE [10] | Ratio of Samples for training | | |
| | 80% | 50% | 30% | | 80% | 50% | 30% |
| LIVE | 0.9528 | 0.9414 | 0.9277 | LIVE | 0.9557 | 0.9410 | 0.9094 |
| CSIQ | 0.8845 | 0.8706 | 0.8605 | CSIQ | 0.9085 | 0.8857 | 0.8628 |
| TID2008 | 0.8990 | 0.8814 | 0.8680 | TID2008 | 0.9085 | 0.8696 | 0.8228 |
| Average | 0.9147 | 0.9009 | 0.8886 | Average | 0.9270 | 0.9035 | 0.8716 |
| BIQI [13] | Ratio of Samples for training | | | QAC | N.A | | |
| | 80% | 50% | 30% | | | | |
| LIVE | 0.8429 | 0.7993 | 0.7484 | LIVE | | 0.8857 | |
| CSIQ | 0.7598 | 0.7208 | 0.6721 | CSIQ | | 0.8627 | |
| TID2008 | 0.8438 | 0.7510 | 0.6778 | TID2008 | | 0.8697 | |
| Average | 0.8123 | 0.7587 | 0.7034 | Average | | 0.8733 | |

*Figure 9* *Computational Complexity compared to other methods.*

# CHAPTER 3

# METHODOLOGY

In this chapter we will discuss all the steps needed from capturing the sample with two types of illuminations, the autofocus MATLAB algorithms and the configuration of the Raspberry Pi to drive the Led Matrix and capture the images. Then we will continue with the physical design of the microscope and some important parts including their features. In the end we will plan our experiment which will be conducted in next chapter and the results we got.

## 3.1    Microscope Preparation

The design of microscopes has evolved over the time. To set up our microscope we purchased most of the parts online, starting from optical table and its components are bought, lenses, filters, sensors, polarizers, beam splitters, illumination sources diffusers and a host of other components. These are professional tools which allows us to customize our microscope.

### 3.1.1    Eyepieces

This part of microscope is needed to produce the base magnification of the image. It is located closest to the eye of the sensor magnifies and projects this real image and yields a virtual image of the object. Eyepiece magnification vary from 1X to 30X but typically they produce a magnification of 10X.[10]

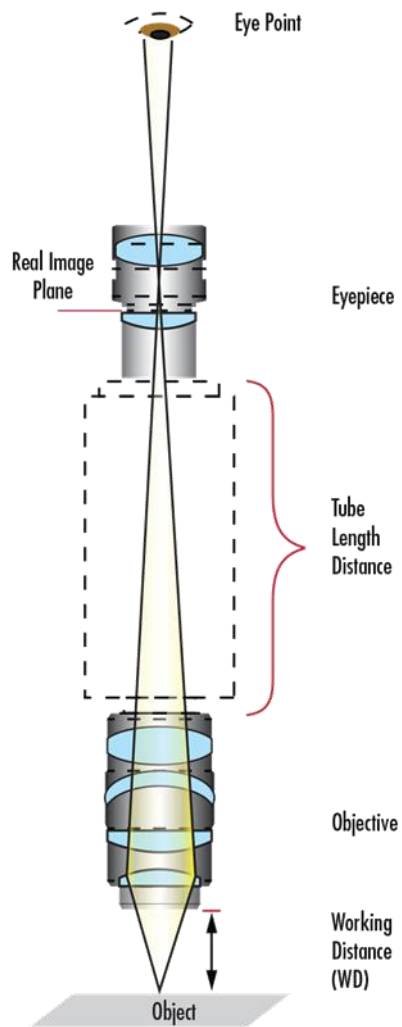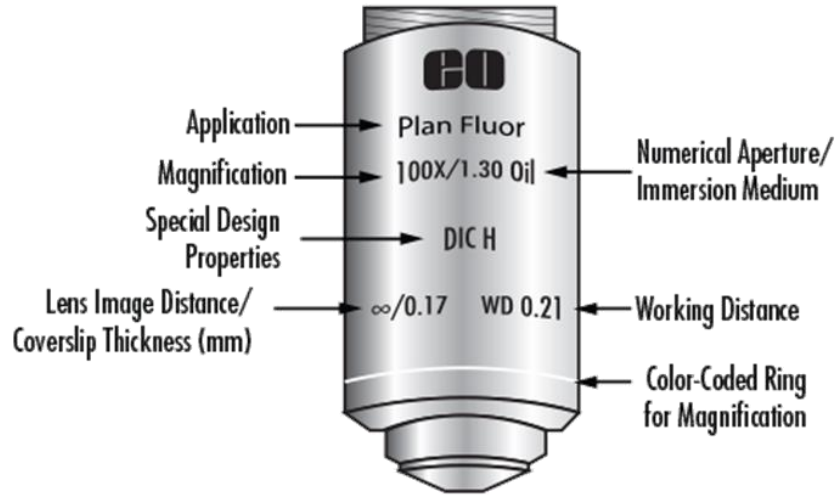**mSystem = mObjective x mEyepiece**   (Equation 15)



***Figure 10***  *Microscope*

### 3.1.2 Magnification

Objectives and eyepieces have magnifications which contribute to the system magnification. It is usually denoted by X next to numerical aperture.



| Magnification | 1X | 2X | 3X | 4X | 10X | 20X | 40X | 60X | 100X |
|---|---|---|---|---|---|---|---|---|---|
| Color Code | Black | Gray | Red | Yellow | Green | Light Blue | Light Blue | Dark Blue | White |

*Figure 11 Microscope*

Numerical aperture (NA) of an objective is a function of focal length and pupil diameter. It is expressed by the following formula:

$$NA = n * sin(theta) \qquad \text{(Equation 16)}$$

Large NA objective sometimes requires usage of immersion oils because the highest NA[11]

that can be achieved within the air is NA=1 (corresponding to 90-degree angle of light). To get a larger angle it is necessary to change the refractive index between the object and the objective.

In this setup we are using brightfield microscopy which requires a change in opacity throughout the object. The object is surrounded by a dark haze created by the illumination. The ultimate result is a picture with a lot of contrast between the object's elements and the light source. Unless the object is exceptionally transparent, the resulting image usually allows the user to see each part of the object with some clarity.

Backlight illumination is used in many microscopes instead of standard direct light illumination because the latter tends to oversaturate the item under investigation. Koehler illumination is a form of backlight illumination used in microscopy applications. Incident light from an illumination source, such as a light bulb, floods the object under investigation with light from behind in Koehler illumination (Figure 2). The collecting lens and the condenser lens are both convex lenses. It's made to offer strong, even illumination on the object plane as well as the image plane, where the picture from the objective is reimaged through the eyepiece.[12] This is significant because it assures that the user is not visualizing the light bulb filament.
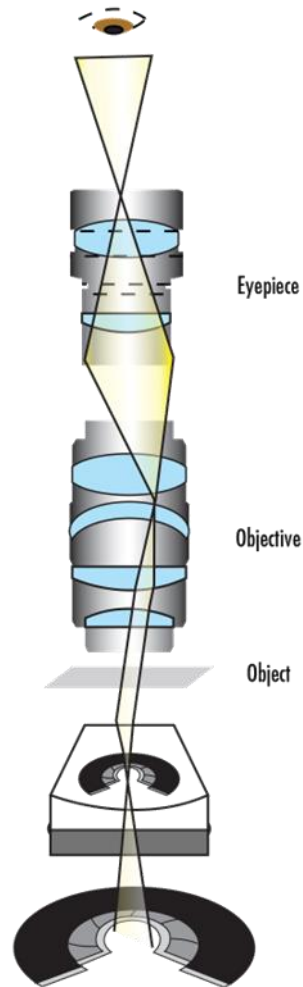
*Figure 12* *Microscpe*

### 3.1.3  Raspberry Pi Configuration

The whole system is driven by a raspberry pi 4 GB Ram memory and 128 GB Rom memory. The project uses a program written in Python 3 (amicro.py) to control the microscope and illumination method in in case when we use led matrix.

### 3.1.4  Autofocus Configuration LabView

The goal of focus measure operators is to determine the sharpness or focus of an image or image pixel. The image on the right was acquired by focusing the camera

27

on the backdrop, but the one on the left was captured by focusing the camera on the foreground object, as seen below. This data is useful for a variety of applications, including autofocusing, image enhancement, and depth estimate based on focus.

Depending on the application, a broad range of techniques and operators have been proposed in the literature to measure the degree of focus of an entire image or an image pixel. The focus measure operators discussed in this chapter have been divided into six major families to make explaining their working principles easier: gradient-based, Laplacian-based, wavelet-based, statistics-based, DCT-based, and miscellaneous operators.[13]
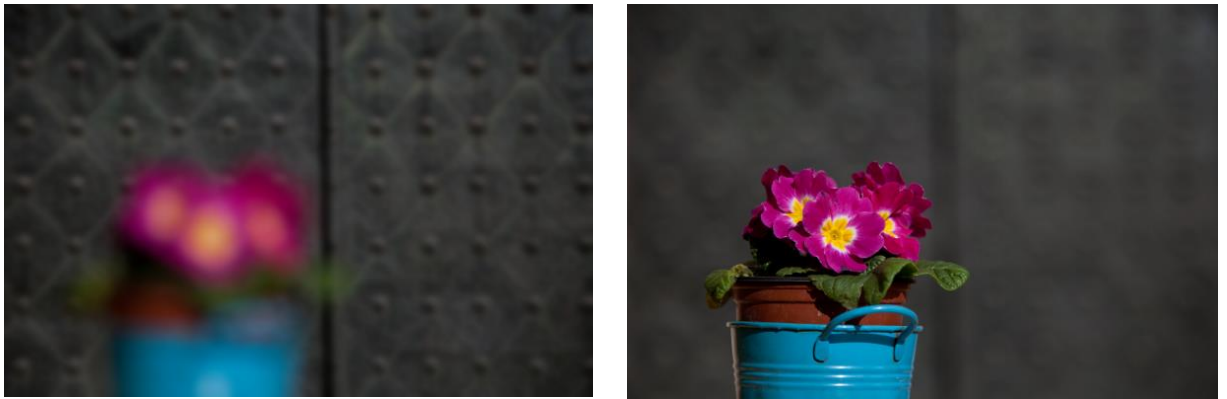


*Figure 13* *Autofocus configuration via labview*

MATLAB code applied is combined with LabView to drive physical parts of the microscope to achieve best in focus image.

Datasets of images are captured in different conditions. We have one dataset where we use Laser illumination as light source of the microscope. The parameters that are change during the experiment setup will be listed on following diagram
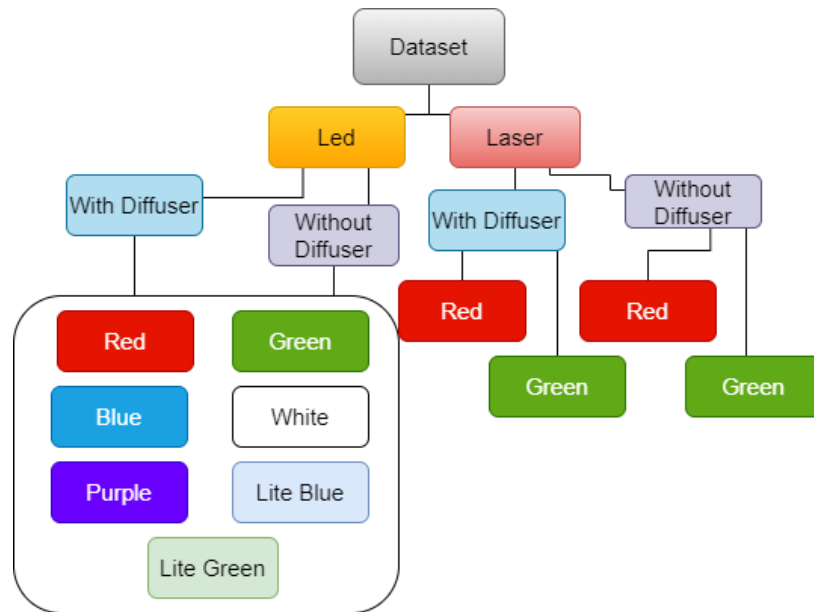
***Figure 14*** *Image Capturing Graph*

# CHAPTER 4

# RESULTS AND DISCUSSIONS

In this section we will discuss the experiments conducted during this work. The aim of these experiments was to determine which of the methods had a better image quality capturing. In total we captured 35 images for our test. All images were captured via microscope using lazer and led illumination source. Some images were also captured using diffusers and different illumination. As test image was used the image below:
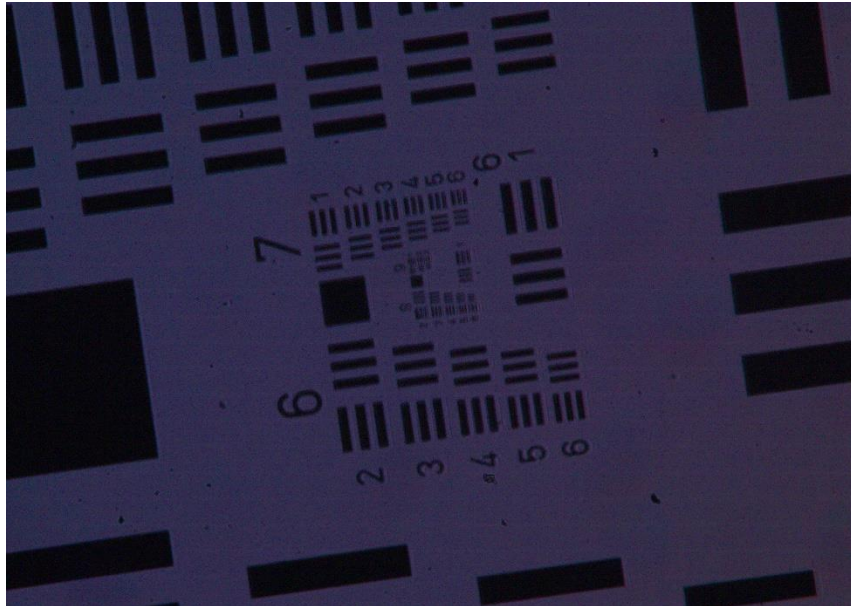


*Figure 15 Sample image used in this experiments USAF 89*

## 4.1 Image Quality Assessment using NIMA Network

The first experiment was conducted using the Neural Image Asessment NIMA network. This network was proposed in 2018 from Hossein Talebi. The network was pre trained using the Aesthetic Visual Analysis dataset. This dataset contained over 250 000 images with a lot of metadata. The dataset contained over 60 categories, semantic labels, and many aesthetic scores for all images. This algorithm NIMA can be used to automatically detect image quality or as loss function to improve image quality, by capturing more images. In this work we use it to evaluate the image quality of our captured images. We have two sets of images, those captured using laser and those captured using the led.

### 4.1.2 Laser Image Assessment using NIMA

In total 8 images were assessed. There were two types of lasers, red and green. For each laser 4 images were captured. Below we show the captured images.
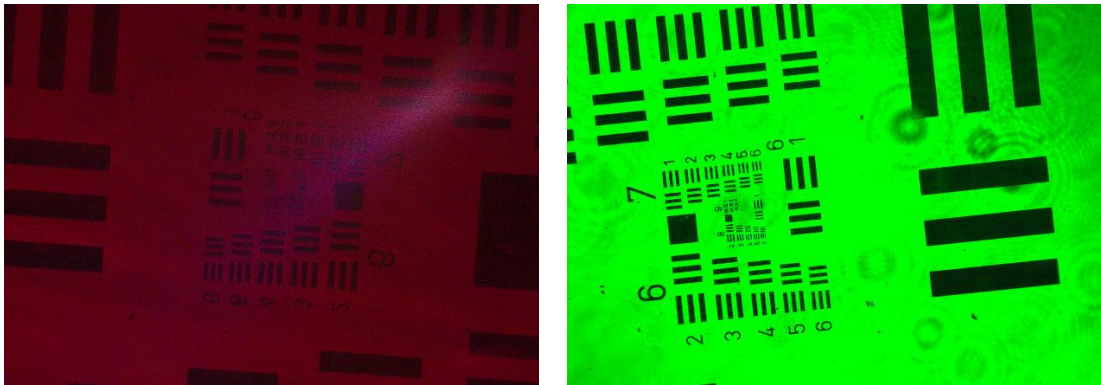


***Figure 16*** *Sample image used in this experiments USAF 89 illuminated with red and green laser.*

The NIMA network implemented in python and pretrained by AVA dataset was called as a separate process for each image and results were saved in text files. In

the end these results were obtained as assessment scores from the algorithm by the master process that called the algorithm for all images obtained by lazer.

*Table 3* *Quality Scores by implementing NIMA network on our dataset.*

| Image | Score |
|---|---|
| Image__2022-05-07__17-47-28.bmp | 4.69958 |
| Image__2022-05-07__17-47-57.bmp | 4.37786 |
| Image__2022-05-07__17-48-11.bmp | 4.75105 |
| Image__2022-05-07__17-48-39.bmp | 5.01075 |
| Image__2022-05-07__17-54-21.bmp | 4.00485 |
| Image__2022-05-07__17-54-35.bmp | 3.87227 |
| Image__2022-05-07__17-54-41.bmp | 3.94053 |
| Image__2022-05-07__17-58-45.bmp | 3.68606 |

The first four images are captured by green laser while the last remaining via red lazer. Overall, what we are interested in here is the mean value of these values. Below we show a chart for this case as a better evaluation for this method. The average accuracy for images obtained via green lazer is 4.70981. For those obtained via red lazer is 3.8759275.
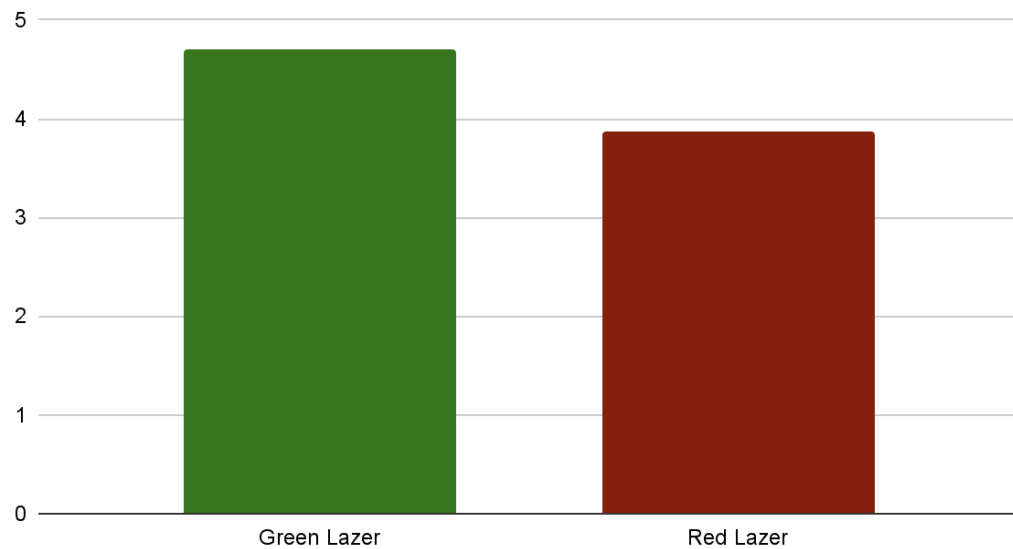
## Mean Image Quality Score



*Table 4 Mean Image Quality score for green and red laser illumination*

As we can see the quality score is higher for the green laser. In total the best quality score was 5.01075 for the lazer. The worst was 3.686 while the mean for images with lazer was 4.29.

### 4.1.3 Led Image Assessment Using NIMA

Images obtained with led were also used for image quality assessment. Science we were able to leverage the light type we tried to capture images on different wavelengths to see how this would affect the quality score and obtain the best results. In total were taken 4 images for each wavelength. 6 Wavelength were considered in total:

- Blue

- Green

- Lite Blue

- Purple

- Red

- White

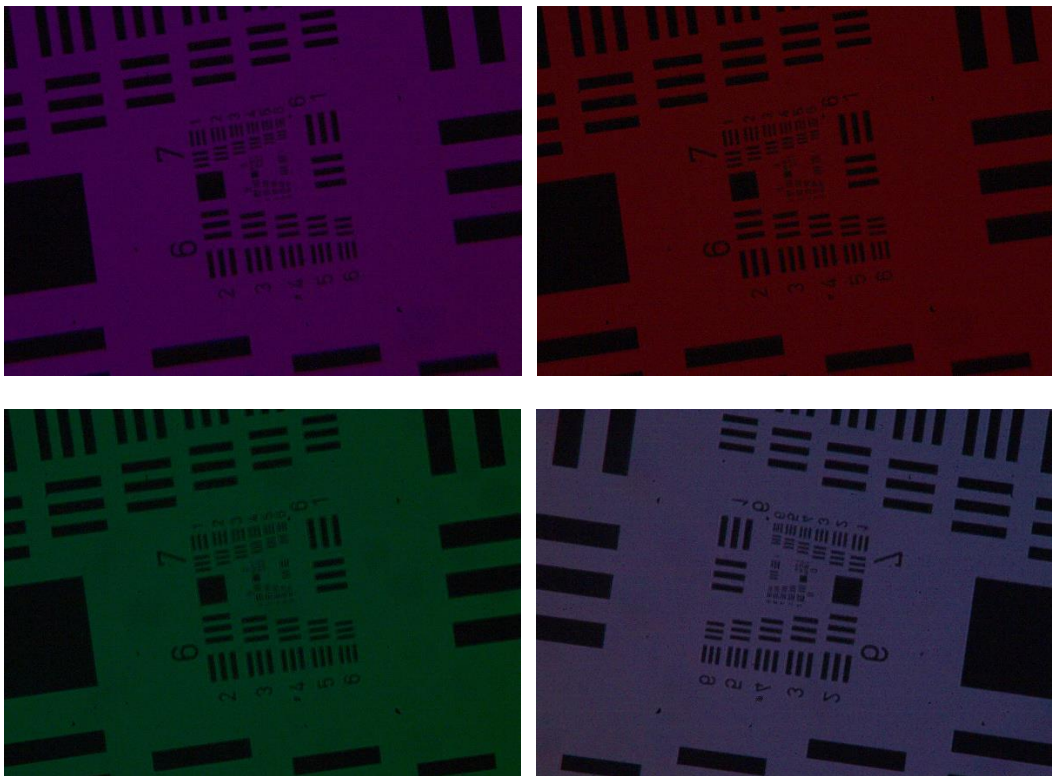These are some of the images obtained by led.



*Figure 17* *Sample image used in this experiments USAF 89 illuminated with purple, red, green, and white laser.*

In total 24 images were obtained. We are going to show a table with the mean values of scores for images obtained from this led below.

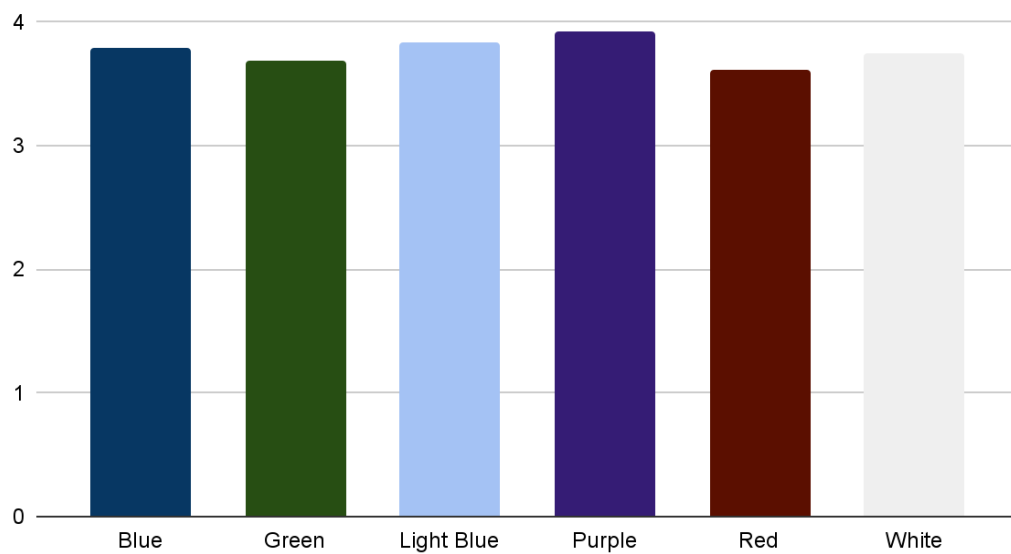| Led Light | Mean Score |
|-----------|------------|
| Blue | 3.79 |
| Green | 3.69 |
| Light Blue | 3.83 |
| Purple | 3.92 |
| Red | 3.62 |
| White | 3.75 |



*Figure 19* *Mean Quality Score for images using different wavelengths.*

An interesting point here is that as wavelength decreases the quality score increases. From Red to Green to Blue ending with Purple. We still need to test images with the other algorithm to define if lower wavelengths give better results or not.

Comparing these results with the previous ones we can say that the lazer has a better performance in capturing images. Checking the bar, we can see that the green laser has the best performance in capturing high quality images. Next is the purple led in led imaging capturing. Then we have the reed lazer followed up by other led images.

## 4.2   BRISQUE Experiment

Images were also assessed using the brisque algorithm. This would help us to compare captured images from different prespectives. We will start with the lazer images. Below we show the table of the values obtained by brisque for each of the lazer images in table.

*Table 5 Below we show the table for all colors for a better visualization.*

| Image | Brisque Score normalized (divided by 10) |
|---|---|
| Image__2022-05-07__17-47-28.bmp | 4.2046 |
| Image__2022-05-07__17-47-57.bmp | 4.8998 |
| Image__2022-05-07__17-48-11.bmp | 4.3268 |
| Image__2022-05-07__17-48-39.bmp | 3.7054 |
| Image__2022-05-07__17-54-21.bmp | 2.014 |
| Image__2022-05-07__17-54-35.bmp | 1.9154 |
| Image__2022-05-07__17-54-41.bmp | 2.0233 |

| Image__2022-05-07__17-58-45.bmp | 7.0463 |
|---|---|

As in the previous case the first four are with green laser while the remaining ones are done via red laser.
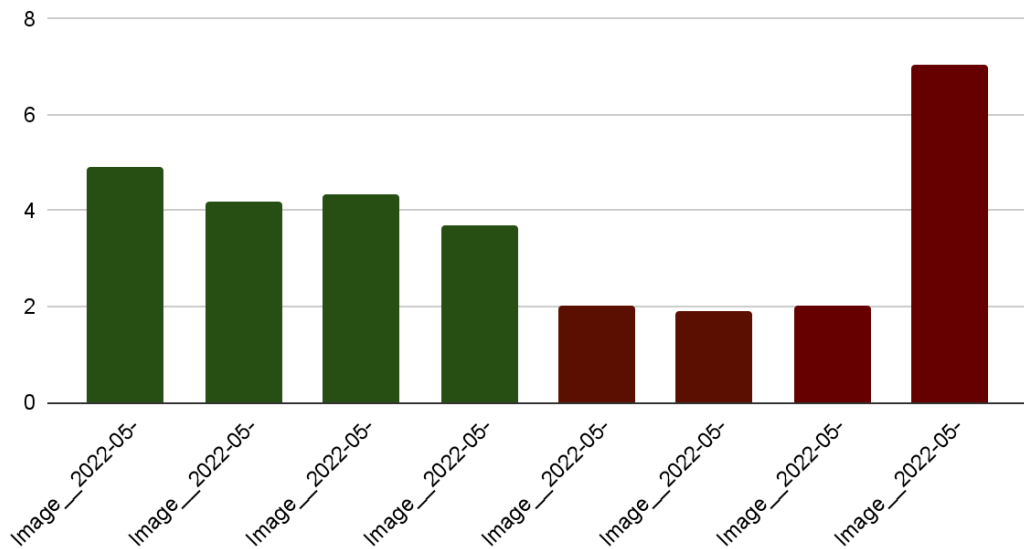


*Figure 20* *Image Quality Scores for Led Images BRISQUE.*

As we can see the lazer images with green lazer have better score with brisque. There is a single image with the highest score with red laser, but science is just only one case it can also be a coincidence. We now build the graph for the images obtained by led. Below we show the table with image led color and the mean score for each image. We divide score by 10 to compare it with the score obtained by the algorithm on the previous sections.

**Table 6** *Mean score for images captured with led using BRISQUE*

| Led Light | Mean Score for Brisque |
|-----------|------------------------|
| Blue | 6.853 |
| Green | 7.5423 |
| Light Blue | 5.625 |
| Purple | 7.826 |
| Red | 7.625 |
| White | 8.211 |

In the upper section we show the results for the light captured images.

# CHAPTER 5

# CONCLUSIONS

## 5.1 Conclusions

In this thesis were compared two types of microscopies which are most popular one nowdays. Laser and LED illumination microscopy is used to achieve high resolution gigapixel images. We compared the quality scores between these two techniques using BRISQUE and NIMA image quality assessments. By comparing the result, we got earlier both techniques have a good performance in quality assessments because we can se similar results between two techniques for the same image, laser and LED illuminated. As we can see from results above *(figure 4)* in laser illuminated images, green light has performed quite well compared to red illumination. We can defend this definition by mentioning that green light wavelength is between 450-600nm while red light wavelength is above 650 nm. Which means by havin a narrow wavelength green illumination provides better resolution as it hits the sample without viggneting the edges.

Talking about LED illuminated images we can state that for both techniques NIMA and BRISQUE purple wavelength performs better than other wavelengths as it doesn't scatter while hitting the sample. Edges are high contrast and not blured.

Overall, the results of these thesis in comparison of LED and Laser illumination techniques, states that Laser illumination has a higher quality assessment score which means higher resolution images.

# Appendix

## Autofocus Algorithm Matlab Function

```matlab
function FM = fmeasure(Image, Measure, ROI)
%This function measures the relative degree of focus of
%an image. It may be invoked as:
%
%   FM = fmeasure(IMAGE, METHOD, ROI)
%
%Where
%   IMAGE,  is a grayscale image and FM is the computed
%           focus value.
%   METHOD, is the focus measure algorithm as a string.
%           see 'operators.txt' for a list of focus
%           measure methods.
%   ROI,    Image ROI as a rectangle [xo yo width heigth].
%           if an empty argument is passed, the whole
%           image is processed.
%
% Said Pertuz
% Jan/2016


if nargin>2 && ~isempty(ROI)
    Image = imcrop(Image, ROI);
end

WSize = 15; % Size of local window (only some operators)

switch upper(Measure)

    % Measure No. 1
    case 'GRAE' % Energy of gradient (Subbarao92a)
        Ix = Image;
        Iy = Image;
        Iy(1:end-1,:) = diff(Image, 1, 1);
        Ix(:,1:end-1) = diff(Image, 1, 2);
        FM = Ix.^2 + Iy.^2;
        FM = mean2(FM);

        % Measure No. 2
    case 'GDER' % Gaussian derivative (Geusebroek2000)
        N = floor(WSize/2);
        sig = N/2.5;
        [x,y] = meshgrid(-N:N, -N:N);
        G = exp(-(x.^2+y.^2)/(2*sig^2))/(2*pi*sig);
        Gx = -x.*G/(sig^2);
        Gx = Gx/sum(abs(Gx(:)));
        Gy = -y.*G/(sig^2);
        Gy = Gy/sum(abs(Gy(:)));
        Rx = imfilter(double(Image), Gx, 'conv', 'replicate');
        Ry = imfilter(double(Image), Gy, 'conv', 'replicate');
        FM = Rx.^2+Ry.^2;
```

```matlab
        FM = mean2(FM);


        % Measure No. 3
    case 'GRAT' % Thresholded gradient (Snatos97)
        Th = 0; %Threshold shold be greater than or equal to 0
        Ix = Image;
        Iy = Image;
        Iy(1:end-1,:) = diff(Image, 1, 1);
        Ix(:,1:end-1) = diff(Image, 1, 2);
        FM = max(abs(Ix), abs(Iy));
        FM(FM<Th)=0;
        FM = sum(FM(:))/sum(sum(FM~=0));


        % Measure No. 4
    case 'GRAS' % Squared gradient (Eskicioglu95)
        Ix = diff(Image, 1, 2);
        FM = Ix.^2;
        FM = mean2(FM);


        % Measure No. 5
    case 'LAPE' % Energy of laplacian (Subbarao92a)
        LAP = fspecial('laplacian');
        % LAP=[1 1 1; 1 -8 1; 1 1 1];
        FM = imfilter(Image, LAP, 'replicate', 'conv');
        FM = mean2(FM.^2);



        % Measure No. 6
    case 'LAPM' % Modified Laplacian (Nayar89)
        M = [-1 2 -1];
        Lx = imfilter(Image, M, 'replicate', 'conv');
        Ly = imfilter(Image, M', 'replicate', 'conv');
        FM = abs(Lx) + abs(Ly);
        FM = mean2(FM);



        % Measure No. 7
    case 'WAVV' %Variance of  Wav...(Yang2003)
        [C,S] = wavedec2(Image, 1, 'db6');
        H = abs(wrcoef2('h', C, S, 'db6', 1));
        V = abs(wrcoef2('v', C, S, 'db6', 1));
        D = abs(wrcoef2('d', C, S, 'db6', 1));
        FM = std2(H)^2+std2(V)+std2(D);


        % Measure No. 8
    case 'WAVR' % Wavelet ratio (Xie2006)
        [C,S] = wavedec2(Image, 3, 'db6');
        H = abs(wrcoef2('h', C, S, 'db6', 1));
        V = abs(wrcoef2('v', C, S, 'db6', 1));
        D = abs(wrcoef2('d', C, S, 'db6', 1));
        A1 = abs(wrcoef2('a', C, S, 'db6', 1));
        A2 = abs(wrcoef2('a', C, S, 'db6', 2));
        A3 = abs(wrcoef2('a', C, S, 'db6', 3));
        A = A1 + A2 + A3;
        WH = H.^2 + V.^2 + D.^2;
```

```matlab
        WH = mean2(WH);
        WL = mean2(A);
        FM = WH/WL;


        % Measure No. 9
    case 'GLVA' % Graylevel variance (Krotkov86)
        FM = std2(Image);



        % Measure No. 10
    case 'HISE' % Histogram entropy (Krotkov86)
        FM = entropy(Image);



        % Measure No. 11
    case 'STD' % standart Deviation
        FM = std2(Image);



        % Measure No. 12
    case 'HISR' % Histogram range (Firestone91)
        FM = max(Image(:))-min(Image(:));



        % Measure No. 13
    case 'CURV' % Image Curvature (Helmli2001)
        if ~isinteger(Image), Image = im2uint8(Image);
        end
        M1 = [-1 0 1;-1 0 1;-1 0 1];
        M2 = [1 0 1;1 0 1;1 0 1];
        P0 = imfilter(Image, M1, 'replicate', 'conv')/6;
        P1 = imfilter(Image, M1', 'replicate', 'conv')/6;
        P2 = 3*imfilter(Image, M2, 'replicate', 'conv')/10 ...
            -imfilter(Image, M2', 'replicate', 'conv')/5;
        P3 = -imfilter(Image, M2, 'replicate', 'conv')/5 ...
            +3*imfilter(Image, M2, 'replicate', 'conv')/10;
        FM = abs(P0) + abs(P1) + abs(P2) + abs(P3);
        FM = mean2(FM);

        % Measure No. 14
    case 'SFRQ' % Spatial frequency (Eskicioglu95)
        Ix = Image;
        Iy = Image;
        Ix(:,1:end-1) = diff(Image, 1, 2);
        Iy(1:end-1,:) = diff(Image, 1, 1);
        FM = mean2(sqrt(double(Iy.^2+Ix.^2)));


    otherwise
        error('Unknown measure %s',upper(Measure))
end
end
%****************************************************************
```

# REFERENCES

[1] S. Shi *et al.*, "Region-Adaptive Deformable Network for Image Quality Assessment," Apr. 2021, [Online]. Available: http://arxiv.org/abs/2104.11599

[2] Y. Xia, C. Sun, and W. X. Zheng, "Discrete-time neural network for fast solving large linear L1 estimation problems and its application to image restoration," *IEEE Transactions on Neural Networks and Learning Systems*, vol. 23, no. 5, pp. 812–820, 2012, doi: 10.1109/TNNLS.2012.2184800.

[3] M. Prabhushankar, D. Temel, and G. Alregib, "MS-UNIQUE: Multi-model and Sharpness-weighted Unsuper-vised Image Quality Estimation."

[4] E. Allen, S. Triantaphillidou, and R. E. Jacobson, "Image Quality Comparison Between JPEG and JPEG2000. I. Psychophysical Investigation," 2007, doi: 10.2352/J.ImagingSci.Technol.200751:3248.

[5] Y. Bengio, "Deep Learning of Representations for Unsupervised and Transfer Learning," 2012. [Online]. Available: http://www.causality.inf.ethz.ch/unsupervised-learning.php

[6] W. Hou, X. Gao, D. Tao, and X. Li, "Blind image quality assessment via deep learning," *IEEE Transactions on Neural Networks and Learning Systems*, vol. 26, no. 6, pp. 1275–1286, Jun. 2015, doi: 10.1109/TNNLS.2014.2336852.

[7] N. Damera-Venkata, T. D. Kite, W. S. Geisler, B. L. Evans, and A. C. Bovik, "Image Quality Assessment Based on a Degradation Model," 2000.

[8] W. Xue, L. Zhang, and X. Mou, "Learning without human scores for blind image quality assessment," in *Proceedings of the IEEE Computer Society Conference on Computer Vision and Pattern Recognition*, 2013, pp. 995–1002. doi: 10.1109/CVPR.2013.133.

[9] W. Xue, L. Zhang, and X. Mou, "Learning without human scores for blind image quality assessment," in *Proceedings of the IEEE Computer Society*

*Conference on Computer Vision and Pattern Recognition*, 2013, pp. 995–1002. doi: 10.1109/CVPR.2013.133.

[10] Z. Wang and A. C. Bovik, "IS IMAGE QUALITY ASSESSMENT SO DIFFICULT?" [Online]. Available: http://anchovy.ece.utexas.eduizwanglrese

[11] W. Hou, X. Gao, D. Tao, and X. Li, "Blind image quality assessment via deep learning," *IEEE Transactions on Neural Networks and Learning Systems*, vol. 26, no. 6, pp. 1275–1286, Jun. 2015, doi: 10.1109/TNNLS.2014.2336852.

[12] S. Bianco, L. Celona, P. Napoletano, and R. Schettini, "On the use of deep learning for blind image quality assessment," *Signal, Image and Video Processing*, vol. 12, no. 2, pp. 355–362, Feb. 2018, doi: 10.1007/s11760-017-1166-8.

[13] H. Talebi and P. Milanfar, "NIMA: Neural Image Assessment," Sep. 2017, doi: 10.1109/TIP.2018.2831899.